# Incorporating System Frequency Dynamics into Real-time Locational Marginal Pricing of Electricity

Bo Chen, *Student Member, IEEE*, Roohallah Khatami, *Member, IEEE*,
Abdullah Al-Digs, *Member, IEEE*, and Yu Christine Chen, *Member, IEEE*

***Abstract*—This paper presents a method to generalize locational marginal prices (LMPs) to embed the impact of system frequency dynamics into real-time electricity markets. The proposed frequency dynamics-aware LMPs can help to mitigate costs associated with setting aside ever more reserve capacity to offset larger, faster, and more frequent transient excursions arising from greater renewable integration. We formulate a dynamics-aware economic dispatch (ED) by augmenting a traditional static ED with constraints pertinent to system frequency dynamics, including those from inertial response, primary frequency control, and the automatic generation control. We show that, similar to their traditional static counterparts, dynamics-aware LMPs are composed of Lagrange multipliers associated with the power balance and transmission line power flow constraints. Furthermore, through analysis, we detail dynamic and steady-state behaviours of dynamics-aware LMPs. Finally, numerical simulations involving standard test systems validate our findings, confirm added revenue opportunities for generators contributing to frequency support, and demonstrate computational scalability.**

***Index Terms*—Automatic generation control, economic dispatch, frequency dynamics, locational marginal pricing**

## I. Introduction

MODERN electric power systems are undergoing revolutionary changes as conventional fossil fuel-based generators are increasingly replaced by low-inertia renewable energy sources (RESs) [1]. The benefits of integrating a greater share of RESs in the generation mix are indisputable for environmental sustainability. However, the variability and intermittency of RESs, coupled with reduced total system inertia, may jeopardize reliable and efficient real-time operation of the power system [2], [3]. A compelling strategy to mitigate this is for (possibly a subset of) RESs to, alongside conventional rotational-inertia sources, contribute to balancing the net demand on a second-to-second basis. Such dispatchable RESs can be realized by equipping their grid-interfacing power-electronic inverters with virtual inertia-based frequency-responsive controllers [4]. Critical to practical deployment of this general strategy is a market-based framework that seamlessly reconciles services provided by inverter-based sources and conventional turbine-based generation and offers suitable compensation, which would then foster further investment into RESs to support real-time operations [5]. Our work is indeed positioned *along* the energy transition marked by the coexistence of renewable and conventional sources.

The overarching aim of electricity markets is to supply the electric load with minimum cost. They typically follow a hierarchical multi-stage structure spanning longer scheduling horizons with coarser trading intervals (e.g., day-ahead market) followed by shorter scheduling horizons with finer trading intervals (e.g., real-time market) [6], [7]. In general, each market stage collects trade terms (bids and offers) from market participants, which are then used to obtain so-called locational marginal prices (LMPs) [8]. The LMP associated with a particular bus in a power system represents the optimal marginal cost incurred to supply an additional unit of electric load at that bus given cost of operation, supply-demand balance, and transmission and generation capacity limits [9].

Real-time LMPs accompany the solution of an electricity pricing problem commonly known as real-time economic dispatch (ED) typically solved every 5 minutes [10]–[12]. The traditional static ED is a single-interval optimization problem formulated under the implicit assumption that the power system operates in steady state over the entire scheduling horizon. Thus, resulting LMPs do not capture the operation cost during frequency transients away from the synchronous steady state. Such excursions are instead addressed by frequency containment (or control) reserves, and reserve requirements are expected to grow rapidly with increasing integration of low-inertia RESs that cause larger, faster, and more frequent frequency deviations [13]. However, providing additional reserves by investing in more fast-acting generating units or curtailing existing ones is not attractive economically. In this paper, we propose real-time *dynamics-aware* LMPs that are valid throughout frequency transients and into steady state by extending the traditional ED into a multi-interval multi-time scale optimization problem. The resulting LMPs updated at shorter intervals represent the actual second-to-second marginal cost of *energy* in regulating system frequency and thereby in tracking net demand variations in real time. While the proposed method departs significantly from today's regulation markets where generators are paid for reserve *capacity* [6], [7], it offers a promising extension of real-time markets to mitigate the greater total operation cost expected from growing reserve requirements as mentioned earlier. Then, having accounted for frequency regulation in the real-time energy market, we envision reserve capacity would instead be procured to offset the risk of constraint violation due to uncertainty in, e.g., the net-load forecast.

Although the proposed dynamics-aware LMPs are solved

Authors are affiliated with the Department of Electrical and Computer Engineering at The University of British Columbia, Vancouver, Canada. E-mail: {cbhp1993, roohallah.khatami, aldigs, chen}@ece.ubc.ca. They gratefully acknowledge the support of the Natural Sciences and Engineering Research Council of Canada (NSERC), funding reference numbers RGPIN-2016-04271 and RGPIN-2023-05240.

alongside a companion ED, this paper is not centered on algorithm design or control synthesis. Instead, we aim to address challenges expected in maintaining cost-effective reliable operations under existing markets, which have motivated recent work in pricing rotational and virtual inertia to mitigate undesired frequency excursions. In [14], a Vickrey-Clarke-Groves mechanism helps to procure sufficient system inertia to withstand worst-case contingencies while minimizing the cost under a performance metric that reflects efficient frequency response. Further, [15], [16] tailor the traditional unit commitment (UC) to jointly optimize the costs of procuring energy and inertia, where the system inertia is informed by requirements for frequency nadir [15] and rate of change of frequency [16]. While [15], [16] derive pertinent performance indices from a mathematical model of system frequency dynamics, [17] uses linear constraints fitted to simulation data. A chance-constrained UC with inertia constraints in [18] co-optimizes the costs of energy and inertia services while accounting for load uncertainty. The aforementioned efforts all target the procurement and pricing of adequate inertia by introducing a *new* service. In contrast, our recent work [19] seeks to extend *existing* real-time markets based in marginal pricing to incorporate contributions made by generators toward restoring the frequency to synchronous steady state after a disturbance. Related work in (locational) marginal pricing address pricing under uncertainty [20], [21], nonconvex pricing [22], [23], and multi-interval pricing [24], [25]. A more detailed review of recent literature on extensions of LMPs can be found in [26]. Also worth mentioning are efforts in optimal frequency-aware scheduling of conventional and inverter-based sources to mitigate undesired frequency excursions (see, e.g., [27]–[29] and references therein). Distinct from these, our focus is squarely on generalizing the concept of LMPs aimed at a more granular-in-time extension of existing real-time markets.

This paper formulates a multi-interval multi-time scale ED that embeds relatively fast frequency dynamics along with slower decisions on generator/inverter set-points into one single optimization problem. We augment the traditional ED with constraints pertinent to frequency dynamics arising from synchronous generators (the model for which straightforwardly generalizes over that for a frequency-responsive inverter controller furnished with virtual inertia and droop characteristics). Distinct from [19] that enables secondary frequency control by penalizing frequency deviations (from synchronous speed) in the objective function, the dynamics-aware ED formulated in this paper more accurately reflects actual system operations by incorporating the dynamical model of the automatic generation control (AGC). We further enforce transmission line power flow limits and account for the effects of congestion on marginal cost. The use of injection shift factors that map nodal power injections to line power flows uncovers *locational* marginal prices, unlike [19] where a single marginal price is shared amongst all buses in the system. We show that the real-time *dynamics-aware* LMPs comprise Lagrange multipliers associated with the generation-load balance and line power flow limits. In examining the dynamics of the LMPs, we derive a state-space model for pertinent Lagrange multipliers of the dynamics-aware ED. Finally, extensive numerical simulations involving standard test cases (namely the Western System Coordinating Council 9-bus, New England 39-bus, and IEEE 145-bus test systems) validate our analysis, demonstrate dynamics in the proposed LMPs, confirm added revenue opportunities for generators, and showcase computational scalability.

The remainder of the paper is organized as follows. Section II outlines pertinent models for the traditional ED, the AGC, and generators. In Section III, we formulate the dynamics-aware ED and present its optimality conditions. Section IV derives the dynamics-aware LMPs and examines their dynamic and steady-state behaviours. Section V comprises numerical simulations to validate and illustrate dynamics in LMPs and the system. Finally, Section VI concludes the paper.

## II. Preliminaries

In this section, we introduce the LMPs solved from a traditional single-snapshot dynamics-oblivious ED. We also outline dynamical models pertinent to the AGC and generators. We further discuss the motivation behind proposing the concept of dynamics-aware LMPs via a numerical example.

### A. Traditional Locational Marginal Prices

Consider a transmission system with $N$ buses, $L$ lines, and $G$ generators collected respectively in sets $\mathcal{N} = \{1, \ldots, N\}$, $\mathcal{L} = \{1, \ldots, L\}$, and $\mathcal{G} = \{1, \ldots, G\}$. Suppose generator $g$ produces steady-state electrical power $P_{g,\circ}$ with cost function $C_g(P_{g,\circ})$, and denote the load forecast at bus $n$ by $P^{\text{load}}_{n,\circ}$. The total cost of generation is $C(P_\circ) = \sum_{g\in\mathcal{G}} C_g(P_{g,\circ})$, where $P_\circ = [P_{1,\circ}, \ldots, P_{G,\circ}]^{\mathrm{T}}$. Collect the load forecasts at all buses in vector $P^{\text{load}}_\circ = [P^{\text{load}}_{1,\circ}, \ldots, P^{\text{load}}_{N,\circ}]^{\mathrm{T}}$. Further define steady-state nodal net power injections $P^{\text{inj}}_\circ := KP_\circ - P^{\text{load}}_\circ$, where the $N \times G$ incidence matrix $K$ maps generators to bus indices. Then the traditional ED can be formulated as

$$\begin{aligned}
\underset{P_\circ}{\text{minimize}} \quad & C(P_\circ) && \text{(1a)}\\
\text{subject to} \quad & \mathbb{1}_G^{\mathrm{T}} P_\circ = \mathbb{1}_N^{\mathrm{T}} P^{\text{load}}_\circ, \quad (\lambda_\circ), && \text{(1b)}\\
& P^{\text{inj}}_\circ = KP_\circ - P^{\text{load}}_\circ, \quad (\rho_\circ), && \text{(1c)}\\
& \underline{F} \le \Psi P^{\text{inj}}_\circ \le \overline{F}, \ (\phi^-_\circ, \phi^+_\circ), && \text{(1d)}\\
& \underline{P} \le P_\circ \le \overline{P}, \quad (\mu^-_\circ, \mu^+_\circ), && \text{(1e)}
\end{aligned}$$

where $\mathbb{1}_G$ and $\mathbb{1}_N$ respectively represent the $G$- and $N$-dimensional vectors of 1s, and $\Psi$ is the $L \times N$ matrix of injection shift factors. Above, the operation cost in (1a) is minimized subject to system generation-load balance in (1b), nodal power balance in (1c), line power flow limits in (1d), and generator capacity limits in (1e). The cost function $C(\cdot)$ is assumed to be strictly convex and monotonically increasing for the range of generator outputs we consider. The LMP at a particular bus represents the change in the optimal cost due to incremental variations in load at that bus. With respect to the problem in (1), the LMPs consist of the Lagrange multiplier of system power balance in (1b) plus a term attributed to transmission line congestion, as follows:

$$\Lambda_\circ = \mathbb{1}_N \lambda^\star_\circ + \Psi^{\mathrm{T}}(\phi^{-\star}_\circ - \phi^{+\star}_\circ), \tag{2}$$

where the superscript $\star$ denotes the value taken by the corresponding variable at the optimal solution. The ED formulation

in (1) and subsequent LMP calculation in (2) are pieced together from popular textbooks [8], [9] as well as references authored by industry stakeholders [10]–[12].

### B. Automatic Generation Control

Let $P_g^{\mathrm{r}}$ and $P_g$ denote respectively the reference set-point and electrical output of generator $g \in \mathcal{G}$; also let $P^{\mathrm{r}} = [P_1^{\mathrm{r}}, \ldots, P_G^{\mathrm{r}}]^{\mathrm{T}}$ and $P = [P_1, \ldots, P_G]^{\mathrm{T}}$. For a single-area power system, generator reference set-points are obtained as

$$P^{\mathrm{r}} = P_\circ + \pi(\xi - \mathbb{1}_G^{\mathrm{T}} P_\circ), \tag{3}$$

where $P_\circ$ comprises the generator economic dispatch set-points and $\pi = [\pi_1, \ldots, \pi_G]^{\mathrm{T}}$ collects the AGC participation factors (chosen such that $\mathbb{1}_G^{\mathrm{T}}\pi = 1$ and $\pi_g \geq 0, \forall\, g \in \mathcal{G}$) [30]. In existing implementations, $P_\circ$ would assume the most recent optimal set-point solved from the traditional ED in (1). Furthermore, in (3), $\xi$ is the AGC state variable modelled by the following dynamics:

$$\tau_{\mathrm{A}}\dot{\xi} = -\xi - \mathrm{ACE} + \mathbb{1}_G^{\mathrm{T}} P, \tag{4}$$

where $\tau_{\mathrm{A}}$ is the AGC time constant and $\mathrm{ACE} = -kb\Delta\omega$ is the area control error (ACE) for a single-area power system. Although we consider a single-area system for simplicity, we can easily extend the AGC model for multiple areas (see, e.g., [31]), at the expense of greater notational burden. The state-space model in (3)–(4) is transcribed from the AGC block diagram in [30, p. 494]. Particularly, (4) represents an integrator for the AGC state $\xi$, and (3) assigns generator set-points proportional to the AGC participation factors in $\pi$. While there are significant variations in industry implementations of the AGC, [32], [33] suggest sampling the ACE and actuating control action every two to four seconds, which serves to inform the duration of the longer time interval in the proposed dynamics-aware ED. Also of note is that AGC dynamics are slower *by design* with $\tau_{\mathrm{A}}$ ranging from $30\,[\mathrm{sec}]$ to minutes [33]. Within the ACE signal, $k < 0$ is a predefined constant scaling factor and $b$ the bias factor for the area, and $\Delta\omega = \omega - \omega_{\mathrm{s}}$, where $\omega$ denotes the prevailing frequency for the area and $\omega_{\mathrm{s}} = 2\pi 60\,[\mathrm{rad/s}]$ is the synchronous speed. While practical setups differ on how $\Delta\omega$ is computed from measurements, for modelling purposes in our paper, we assume that it follows dynamics outlined next.

### C. Generator Frequency Dynamics

For each generator $g \in \mathcal{G}$, let $\omega_g$ and $P_g^{\mathrm{m}}$ denote the electrical angular frequency and turbine mechanical power, respectively. Each generator initially operates at the steady-state equilibrium point with $\omega_g(0) = \omega_{\mathrm{s}}$, $P_g^{\mathrm{r}}(0) = P_g^{\mathrm{m}}(0) = P_g(0) = P_g^{\mathrm{r}\circ}$. Let $\Delta\omega_g := \omega_g - \omega_{\mathrm{s}}$ and assume that the electrical distances between geographically different parts of the power system are negligible, then all generator frequencies follow the same transient behaviour, i.e., $\Delta\omega_g = \Delta\omega$, $\forall\, g \in \mathcal{G}$ [34]. Also let $P^{\mathrm{m}} = [P_1^{\mathrm{m}}, \ldots, P_G^{\mathrm{m}}]^{\mathrm{T}}$. Then system frequency dynamics can be modelled as

$$M\Delta\dot{\omega} = P^{\mathrm{m}} - D\Delta\omega - P, \tag{5}$$

$$\tau\dot{P}^{\mathrm{m}} = P^{\mathrm{r}} - P^{\mathrm{m}} - R^{-1}\mathbb{1}_G\Delta\omega, \tag{6}$$

TABLE I: (Example 1). Dynamical model parameters of generators and governors in the WSCC test system (boldface delineates values that *differ* from the standard test case).

| Generator | Case(s) | $M_g$ [sec] | $D_g$ | $\tau_g$ [sec] | $R_g^{-1}$ |
|---|---|---|---|---|---|
| $g = 1$ | 1, 2, 3 | 23.64 | 20 | 2 | 100 |
| $g = 2$ | 1, 2, 3 | 6.4 | 20 | 2 | 100 |
| $g = 3$ | 1 | 3.01 | 20 | 2 | **0** |
| | 2 | 3.01 | 20 | 2 | 100 |
| | 3 | **13.01** | **50** | 2 | **125** |

where $M = [M_1, \ldots, M_G]^{\mathrm{T}}$ and $D = [D_1, \ldots, D_G]^{\mathrm{T}}$ respectively collect the generator inertia and damping constants, and $\tau = \mathrm{diag}([\tau_1, \ldots, \tau_G])$ and $R^{-1} = \mathrm{diag}([R_1^{-1}, \ldots, R_G^{-1}])$ collect the generator governor time constants and inverse-droop constants, respectively [35]. The model in (5)–(6) does not describe dynamics for the generator terminal voltage, automatic voltage regulators, or power system stabilizers. However, we find this model to be *sufficiently accurate* to capture system frequency dynamics for the time scales of our interest [34], [36]. Although, as defined above, each entry in (5)–(6) is constructed for a single generator, it can also serve as an aggregate power plant model fashioned with aggregate values for inertia, damping, and droop constants. Furthermore, this model generalizes over the active-power loop of the so-called *virtual synchronous generator* controller that is commonly adopted in the literature to enable frequency support by inverter-based sources (see, e.g., [37], [38]). Inverter inner-loop voltage and current controller dynamics are neglected as they would be executed at much faster time scales [39].

### D. Motivation for Proposed Dynamics-aware LMPs

The traditional ED in (1) implicitly assumes that the power system operates at synchronous steady state, so resulting LMPs in (2) do not offer any insights on the price of electricity during frequency transients. Thus, traditional LMPs do not incentivize or compensate generators to contribute to dynamic frequency response, a shortcoming that we exemplify next.

**Example 1** (3-Generator 9-Bus System)**.** Consider the Western System Coordinating Council (WSCC) test system [40] with two relatively cheap units and a third more expensive unit. The optimal dispatch from the traditional ED in (1) yields zero output from generator 3, as shown by the initial steady-state operating point in Fig. 1a. Traditionally, the LMPs at which units are compensated are *fixed* assuming the system operates in steady state. We now examine dynamics in generator power and system frequency in response to a $20\%$ increase in all loads imposed at time $t = 10\,[\mathrm{sec}]$, under three different sets of values taken by generator parameters, as reported in Table I. In cases 1 and 2, we use the parameter values from the standard test case, *except* generator 3 sets $R_3^{-1}$ to be identically zero in case 1 but to take a positive value in case 2. We plot the realized mechanical power output of generator 3 in Fig. 1a and system frequency response in Fig. 1b. Since generator 3 does not participate in primary frequency response in case 1, its output remains at zero throughout the simulation period, as shown by the solid trace in Fig. 1a.

Although case 1 is consistent with the steady-state assumption under which optimal dispatch from the traditional ED is

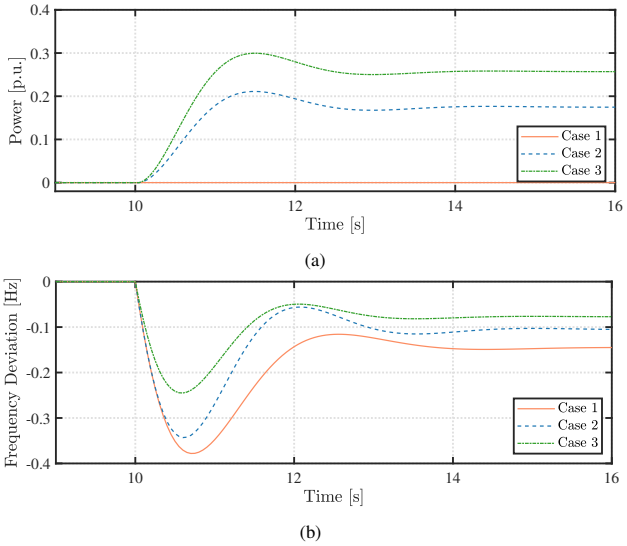


Fig. 1: (Example 1). Dynamic trajectories realized with three different sets of generator parameter values in response to a load increase: (a) mechanical power outputs of the most expensive unit $P_3^{\mathrm{m}}(t)$, (b) system frequency deviations. In case 1, the most expensive unit does not participate in primary frequency response; in case 2, this unit contributes to primary frequency control, resulting in more desirable frequency response; in case 3, parameter values are chosen to achieve even better system frequency response with respect to nadir, settling time, and steady-state deviation.

solved, in examining Fig. 1b, we observe that case 2 depicted by the dashed trace represents more desirable behaviour with i) higher frequency nadir, ii) shorter settling time, and iii) less steady-state deviation from synchronous speed. Following this train of thought, case 3 is engineered with a set of values for inertia, damping, and droop constants for generator 3 that leads to even better system frequency response, as shown by the dash-dot traces in Fig. 1b. ■

In the above example, we observe that different values taken by tuneable controller parameters of conventional generators (and inverter-based sources) can lead to significantly improved dynamic performance. Indeed, due to the expected integration of intermittent renewable generation and reduction in system inertia, generation-load imbalances in the future may lead to larger, faster, and more frequent frequency variations. However, conventional generators participating in frequency response services are largely compensated for setting aside reserve capacity only, not for response speed [29]. Furthermore, at present, inverter-based sources that can potentially provide faster response to generation-load imbalances do not contribute to system inertial or primary frequency response [41]. To address this issue, we generalize traditional static LMPs to incorporate effects of frequency dynamics toward incentivizing conventional generators and inverter-based sources to contribute to frequency response. The proposed method provides a systematic pricing approach rooted in present industry standard practices to compensate generating units over time scales pertinent to inertial response, primary frequency response, and secondary frequency control.

## III. Dynamics-aware Economic Dispatch

The dynamics-aware ED aims to optimize the generation schedule of generator $g \in \mathcal{G}$ over the scheduling horizon of interest, with the system frequency dynamics explicitly modelled. This calls for combining slower decisions on generator reference set-points and comparatively faster frequency dynamics into a *single* multi-time scale optimization problem.

### A. Problem Formulation

Consider the scheduling horizon of the ED problem from time $t_0$ to $t_0 + T$, with $T$ being, e.g., $5\,[\mathrm{min}]$ for real-time markets. Within the ED scheduling horizon, we introduce two pertinent time steps to capture frequency dynamics arising from the AGC and generators. First, AGC decisions on generator reference set-points are made over a longer time interval $\Delta t^{\mathrm{S}}$ (e.g., $5\,[\mathrm{sec}]$), which subdivides the scheduling horizon into equal intervals with the interval endpoints collected in $\mathcal{T}_{t_0}^{\mathrm{S}} = \{t_0, t_0 + \Delta t^{\mathrm{S}}, \ldots, t_0 + T\}$. Next, the time step corresponding to faster frequency dynamics is denoted by $\Delta t^{\mathrm{D}}$ (e.g., $0.05\,[\mathrm{sec}]$), which is sufficiently small to capture the dynamic behaviour of generators. The scheduling horizon then divides into equal intervals with the interval endpoints collected in the set $\mathcal{T}_{t_0}^{\mathrm{D}} = \{t_0, t_0 + \Delta t^{\mathrm{D}}, \ldots, t_0 + T\}$.

We formulate a dynamics-aware ED with fast decisions made every $\Delta t^{\mathrm{D}}$ seconds, slower generator set-points determined every $\Delta t^{\mathrm{S}}$ seconds, and one set of ED set-points applied across the entire scheduling horizon. Considering the forecasted nodal loads collected in $P_t^{\mathrm{load}} = [P_{1,t}^{\mathrm{load}}, \ldots, P_{N,t}^{\mathrm{load}}]^{\mathrm{T}}$, $t \in \mathcal{T}_{t_0}^{\mathrm{D}}$, over the scheduling horizon from $t_0$ to $t_0 + T$, the dynamics-aware ED is formulated as follows:[1]

$$\underset{\substack{P_\circ, \xi_{t'}, P_{t'}^{\mathrm{r}}, P_t^{\mathrm{m}},\\ \Delta\omega_t, P_t, P_t^{\mathrm{inj}}}}{\text{minimize}} \sum_{t \in \mathcal{T}_{t_0}^{\mathrm{D}}} C(P_t^{\mathrm{m}}) \Delta t^{\mathrm{D}} \tag{7a}$$

$$\text{subject to } M\Big(\frac{\Delta\omega_{t+\Delta t^{\mathrm{D}}} - \Delta\omega_t}{\Delta t^{\mathrm{D}}}\Big) = P_t^{\mathrm{m}} - D\Delta\omega_t - P_t, \quad (\alpha_t),\ t \in \mathcal{T}_{t_0}^{\mathrm{D}} \setminus \{t_0 + T\}, \tag{7b}$$

$$\tau\Big(\frac{P_{t+\Delta t^{\mathrm{D}}}^{\mathrm{m}} - P_t^{\mathrm{m}}}{\Delta t^{\mathrm{D}}}\Big) = P_{t'}^{\mathrm{r}} - P_t^{\mathrm{m}} - R^{-1}\mathbb{1}_G\Delta\omega_t, \quad (\beta_t),\ t' \in \mathcal{T}_{t_0}^{\mathrm{S}} \setminus \{t_0 + T\}, \quad t \in \{t', \ldots, t' + \Delta t^{\mathrm{S}} - \Delta t^{\mathrm{D}}\}, \tag{7c}$$

$$\tau_{\mathrm{A}}\Big(\frac{\xi_{t'+\Delta t^{\mathrm{S}}} - \xi_{t'}}{\Delta t^{\mathrm{S}}}\Big) = -\xi_{t'} + kb\Delta\omega_{t'} + \mathbb{1}_G^{\mathrm{T}} P_{t'}, \quad (\gamma_{t'}),\ t' \in \mathcal{T}_{t_0}^{\mathrm{S}} \setminus \{t_0 + T\}, \tag{7d}$$

$$P_{t'}^{\mathrm{r}} = P_\circ + \pi(\xi_{t'} - \mathbb{1}_G^{\mathrm{T}} P_\circ),\ (\kappa_{t'}),\ t' \in \mathcal{T}_{t_0}^{\mathrm{S}}, \tag{7e}$$

$$\mathbb{1}_G^{\mathrm{T}} P_t = \mathbb{1}_N^{\mathrm{T}} P_t^{\mathrm{load}},\ (\lambda_t),\ t \in \mathcal{T}_{t_0}^{\mathrm{D}}, \tag{7f}$$

$$P_t^{\mathrm{inj}} = KP_t - P_t^{\mathrm{load}},\ (\rho_t),\ t \in \mathcal{T}_{t_0}^{\mathrm{D}}, \tag{7g}$$

$$\mathbb{1}_G^{\mathrm{T}} P_\circ = \frac{1}{|\mathcal{T}_{t_0}^{\mathrm{D}}|} \sum_{t \in \mathcal{T}_{t_0}^{\mathrm{D}}} \mathbb{1}_N^{\mathrm{T}} P_t^{\mathrm{load}},\ (\zeta), \tag{7h}$$

$$\underline{F} \le \frac{1}{|\mathcal{T}_{t_0}^{\mathrm{D}}|} \sum_{t \in \mathcal{T}_{t_0}^{\mathrm{D}}} \Psi P_t^{\mathrm{inj}} \le \overline{F},\ (\phi^-, \phi^+), \tag{7i}$$

$$\underline{P} \le P_t^{\mathrm{m}} \le \overline{P},\ (\mu_t^-, \mu_t^+),\ t \in \mathcal{T}_{t_0}^{\mathrm{D}}, \tag{7j}$$

[1] Subscripts $t$ and $t'$ respectively denote variables evaluated at the faster and slower time scales; superscripts D and S respectively represent variables pertinent to the shorter and the longer time intervals; variables related to generator power include electrical output $P_t$, turbine mechanical power $P_t^{\mathrm{m}}$, reference power set-point $P_{t'}^{\mathrm{r}}$, and economic dispatch set-point $P_\circ$; and variables related to nodal power include the load $P_t^{\mathrm{load}}$ and net injection $P_t^{\mathrm{inj}}$.

where $|\cdot|$ is the cardinality operator. The objective in (7a) comprises operation cost $C(P_t^{\mathrm{m}}) = \sum_{g\in\mathcal{G}} C_g(P_{g,t}^{\mathrm{m}})$, where $C_g(\cdot)$ is the cost function for generator $g \in \mathcal{G}$. Approximate discrete-time system dynamics are enforced in (7b)–(7e), where the generator and AGC dynamics are respectively discretized at shorter intervals of $\Delta t^{\mathrm{D}}$ and longer intervals of $\Delta t^{\mathrm{S}}$. The system generation-load balance is imposed in (7f) for each time step, and the nodal power injections are defined in (7g). The sum of ED set-points balances the average system load forecast over the scheduling horizon in (7h). Average transmission line flows are confined to their lower and upper limits in (7i). Note that the use of average flows permits short-term violations of line-flow limits during frequency transients. Generator mechanical powers are subject to box limits in (7j).

We note that the problem in (7) is similar to [27], except the problem formulated in [27] shares the same larger discretization time step as that used for slower generator set-points decisions, thus potentially overlooking faster generator and frequency dynamics. Also, constraints placed on generator ramping rates in [27] (and other similar multi-intervals EDs) to mimic physical limitations of generators are not needed in (7) as it explicitly models faster generator and controller dynamics. Moreover, unlike the emphasis on optimal dynamics-aware dispatch in [27], we focus squarely on generalizing the concept of LMPs to incorporate the effects of generator inertial response along with primary and secondary frequency control, which are traditionally decoupled from marginal pricing.

**Remark 1** (Discretization Methods)**.** The multi-time scale discrete-time dynamical model in (7b)–(7d) is synthesized from a first-order approximation of the continuous-time dynamics in (4)–(6). The proposed dynamics-aware ED is general in the sense that (7) can easily embed discrete-time dynamical models resulting from other (and potentially more accurate) discretization methods, such as the zero-order hold or Tustin approximation. The main benefit of using the first-order approximation is that we can retain the physical system parameters in closed form throughout the analysis of the dual problem leading to the dynamics-aware LMPs in Section IV. Also, via dynamic simulations of standard test cases, we find that the discretization time steps that we consider in numerical case studies presented in Section V yield sufficiently accurate discrete-time dynamical models. In practice, other discretization methods may be preferable depending on requirements for model accuracy and limitations in computational resources. ■

**Remark 2** (Inverter-based Sources)**.** The dynamics-aware ED in (7) can accommodate frequency support from inverter-based sources by incorporating their operation cost in the objective and virtual synchronous generator dynamics in the constraints. Particularly, the operation cost of renewable sources is typically modelled as zero or a linear function of power output [42], neither of which would change the general structure of (7) if implemented into the objective. Also, as mentioned in Section II-C, a well-studied way to perform frequency regulation in grid-tied inverters is to modulate the controller reference set-points to mimic a synchronous generator with virtual inertia and damping coefficients [38]. This model can be incorporated into (7b)–(7c) in a straightforward manner. ■

**Remark 3** (Transmission Losses)**.** In (7), transmission losses are implicitly embedded within the load forecast $P_t^{\mathrm{load}}$. However, straightforward modification of (7) can accommodate loss models typically used in the traditional ED. For example, a common model expresses transmission losses as a quadratic function of generator outputs [8], thereby modifying the system generation-load balance constraint in (7f) as

$$\mathbb{1}_G^{\mathrm{T}} P_t = \mathbb{1}_N^{\mathrm{T}} P_t^{\mathrm{load}} + P_t^{\mathrm{T}} B P_t, \tag{8}$$

where $B$ contains so-called *loss coefficients*, with other parts of (7) remaining unchanged. Other related loss models can be employed in a similar fashion by modifying (7f). ■

### *B. Optimal Lagrangian and Optimality Conditions*

The optimality conditions are expressed through Karush-Kuhn-Tucker (KKT) conditions derived from the Lagrangian of the dynamics-aware ED in (7), as follows:

$$\begin{aligned}
\mathcal{L} = &\sum_{t\in\mathcal{T}_{t_0}^{\mathrm{D}}} \Big( C(P_t^{\mathrm{m}})\Delta t^{\mathrm{D}} + \mu_t^{-\mathrm{T}}(\underline{P} - P_t^{\mathrm{m}}) + \mu_t^{+\mathrm{T}}(P_t^{\mathrm{m}} - \overline{P}) \\
&+ \lambda_t(\mathbb{1}_N^{\mathrm{T}} P_t^{\mathrm{load}} - \mathbb{1}_G^{\mathrm{T}} P_t) + \rho_t^{\mathrm{T}}(P_t^{\mathrm{inj}} - K_t P_t + P_t^{\mathrm{load}}) \Big) \\
&+ \sum_{t'\in\mathcal{T}_{t_0}^{\mathrm{S}}} \kappa_{t'}^{\mathrm{T}}(P_{t'}^{\mathrm{r}} - P_\circ - \pi(\xi_{t'} - \mathbb{1}_G^{\mathrm{T}} P_\circ)) \\
&+ \sum_{t\in\mathcal{T}_{t_0}^{\mathrm{D}}\setminus\{t_0+T\}} \Big( \alpha_t^{\mathrm{T}} \Big( M\Big(\frac{\Delta\omega_{t+\Delta t^{\mathrm{D}}} - \Delta\omega_t}{\Delta t^{\mathrm{D}}}\Big) - P_t^{\mathrm{m}} + D\Delta\omega_t + P_t \Big) \\
&+ \beta_t^{\mathrm{T}} \Big( \tau\Big(\frac{P_{t+\Delta t^{\mathrm{D}}}^{\mathrm{m}} - P_t^{\mathrm{m}}}{\Delta t^{\mathrm{D}}}\Big) - P_{t'}^{\mathrm{r}} + P_t^{\mathrm{m}} + R^{-1}\mathbb{1}_G\Delta\omega_t \Big) \Big) \\
&+ \sum_{t'\in\mathcal{T}_{t_0}^{\mathrm{S}}\setminus\{t_0+T\}} \gamma_{t'} \Big( \tau_{\mathrm{A}}\Big(\frac{\xi_{t'+\Delta t^{\mathrm{S}}} - \xi_{t'}}{\Delta t^{\mathrm{S}}}\Big) + \xi_{t'} - kb\Delta\omega_{t'} - \mathbb{1}_G^{\mathrm{T}} P_{t'} \Big) \\
&+ \phi^{-\mathrm{T}}\Big(\underline{F} - \frac{1}{|\mathcal{T}_{t_0}^{\mathrm{D}}|}\sum_{t\in\mathcal{T}_{t_0}^{\mathrm{D}}} \Psi P_t^{\mathrm{inj}}\Big) + \phi^{+\mathrm{T}}\Big(\frac{1}{|\mathcal{T}_{t_0}^{\mathrm{D}}|}\sum_{t\in\mathcal{T}_{t_0}^{\mathrm{D}}} \Psi P_t^{\mathrm{inj}} - \overline{F}\Big) \\
&+ \zeta\Big(\frac{1}{|\mathcal{T}_{t_0}^{\mathrm{D}}|}\sum_{t\in\mathcal{T}_{t_0}^{\mathrm{D}}} \mathbb{1}_N^{\mathrm{T}} P_t^{\mathrm{load}} - \mathbb{1}_G^{\mathrm{T}} P_\circ\Big).
\end{aligned} \tag{9}$$

Denote the optimal Lagrangian and the optimal decisions of the problem in (7) by, respectively, $\mathcal{L}^\star$ and $\{P_\circ^\star, \xi_{t'}^\star, P_{t'}^{\mathrm{r}\star}, P_t^{\mathrm{m}\star}, \Delta\omega_t^\star, P_t^\star, P_t^{\mathrm{inj}\star}\}_{t\in\mathcal{T}_{t_0}^{\mathrm{D}},\, t'\in\mathcal{T}_{t_0}^{\mathrm{S}}}$. Also let Lagrange multipliers evaluated at the optimal solution be distinguished with superscript $\star$. As an example, $\lambda_t^\star$ represents the optimal value of $\lambda_t$. The optimal solution respects primal feasibility delineated by (7b)–(7j), stationarity conditions, and complementary slackness conditions. Here, we provide two stationarity conditions

$$\mathbb{0}_G = \frac{\partial\mathcal{L}^\star}{\partial P_\circ^\star} = \sum_{t'\in\mathcal{T}_{t_0}^{\mathrm{S}}} (\mathbb{1}_G\pi^{\mathrm{T}}\kappa_{t'}^\star - \kappa_{t'}^\star) - \mathbb{1}_G\zeta^\star, \tag{10}$$

$$\mathbb{0}_N = \frac{\partial\mathcal{L}^\star}{\partial P_t^{\mathrm{inj}\star}} = \frac{1}{|\mathcal{T}_{t_0}^{\mathrm{D}}|}\Psi^{\mathrm{T}}(\phi^{+\star} - \phi^{-\star}) + \rho_t^\star,\ t\in\mathcal{T}_{t_0}^{\mathrm{D}}, \tag{11}$$

which will be useful in the next section. Remaining optimality conditions are reported in Appendix A for completeness.

## IV. Dynamics-aware Locational Marginal Prices

This section presents the main results of the paper pertaining to the proposed dynamics-aware LMPs, which represent the system marginal operation cost due to an incremental change in nodal load while satisfying static and dynamic constraints. Based on this definition, we find that the dynamics-aware LMPs consist of similar constituent components as their dynamics-oblivious counterparts in (2).

**Theorem 1.** Given the optimal Lagrangian $\mathcal{L}^\star$ of the dynamics-aware ED in (7) and its optimal solution $\{P_\circ^\star, \xi_{t'}^\star, P_{t'}^{\mathrm{r}\star}, P_t^{\mathrm{m}\star}, \Delta\omega_t^\star, P_t^\star, P_t^{\mathrm{inj}\star}\}_{t\in\mathcal{T}_{t_0}^{\mathrm{D}},\, t'\in\mathcal{T}_{t_0}^{\mathrm{S}}}$, we calculate the dynamics-aware LMPs as

$$\Lambda_t = \frac{1}{\Delta t^{\mathrm{D}}}\Big(\mathbb{1}_N\lambda_t^\star + \frac{1}{|\mathcal{T}_{t_0}^{\mathrm{D}}|}\Psi^{\mathrm{T}}(\phi^{-\star}-\phi^{+\star})\Big),\ t\in\mathcal{T}_{t_0}^{\mathrm{D}}. \quad (12)$$

*Proof.* By definition, LMPs are calculated as

$$\Lambda_t := \frac{1}{\Delta t^{\mathrm{D}}}\frac{\partial\mathcal{L}^\star}{\partial P_t^{\mathrm{load}}}, \quad (13)$$

where scaling by $\Delta t^{\mathrm{D}}$ removes their dependence on $\Delta t^{\mathrm{D}}$ and results in units consistent with the cost function. From the optimal Lagrangian in (9), (13) evaluates as

$$\Lambda_t = \frac{1}{\Delta t^{\mathrm{D}}}\Big(\mathbb{1}_N\lambda_t^\star + \rho_t^\star + \frac{1}{|\mathcal{T}_{t_0}^{\mathrm{D}}|}\mathbb{1}_N\zeta^\star\Big),\ t\in\mathcal{T}_{t_0}^{\mathrm{D}}. \quad (14)$$

To simplify (14), we shift our attention to (10), the structural properties of which lead to

$$\sum_{t'\in\mathcal{T}_{t_0}^{\mathrm{S}}}\kappa_{t'}^\star = \mathbb{1}_G\overline{\kappa}^\star, \quad (15)$$

where $\overline{\kappa}^\star\in\mathbb{R}$ is a scalar quantity. Next substitute (15) into (10) to get

$$\mathbb{0}_G = (\mathbb{1}_G\pi^{\mathrm{T}}\mathbb{1}_G - \mathbb{1}_G)\overline{\kappa}^\star - \mathbb{1}_G\zeta^\star. \quad (16)$$

Further recognizing that $\pi^{\mathrm{T}}\mathbb{1}_G = 1$, we get $\zeta^\star = 0$. Finally, substitution of $\zeta^\star = 0$ and $\rho_t^\star = -\frac{1}{|\mathcal{T}_{t_0}^{\mathrm{D}}|}\Psi^{\mathrm{T}}(\phi^{+\star}-\phi^{-\star})$ (from (11)) into (14) yields (12), as desired. □

The solution of (7) yields LMPs in (12) at each time step $t\in\mathcal{T}_{t_0}^{\mathrm{D}}$. However, such high-resolution LMPs may challenge present-day granularity of financial settlements to generators. In practice, one way to bridge this gap is to sample the LMPs from (12) at and to hold them constant over a longer time interval that satisfies potential limitations in market settlements or measurement technologies while striking a balance with fair compensation for generator dynamic performance.

### A. Steady State for LMPs

Under normal operation, the combination of governor control and the AGC ensures that the system converges to synchronous steady state after a change in load or generation [31]. Correspondingly, to promote pricing transparency, the marginal cost reflected by the dynamics-aware LMPs ought to also settle to steady state [43]. However, the multi-time scale dynamics-aware ED may, in fact, render steady-state Lagrange multipliers (and thereby steady-state LMPs) mathematically infeasible. Next, for the specific setting of nonbinding inequality constraints at steady state and adequate AGC participation from all generators, we provide a necessary condition for there to exist steady-state Lagrange multipliers from the dynamics-aware ED. For notational consistency, we denote steady-state values of corresponding variables by subscript ss.

**Proposition 1.** Suppose there exists $t_{\mathrm{ss}}^{\mathrm{D}}\in\mathcal{T}_{t_0}^{\mathrm{D}}$ such that for all $t\in\{t_{\mathrm{ss}}^{\mathrm{D}}+\Delta t^{\mathrm{D}},\dots,t_0+T\}$, Lagrange multipliers reach steady state with $\lambda_t^\star = \lambda_{t-\Delta t^{\mathrm{D}}}^\star = \lambda_{\mathrm{ss}}^\star$, $\alpha_t^\star = \alpha_{t-\Delta t^{\mathrm{D}}}^\star = \alpha_{\mathrm{ss}}^\star$, $\beta_t^\star = \beta_{t-\Delta t^{\mathrm{D}}}^\star = \beta_{\mathrm{ss}}^\star$, $\mu_t^{+\star} = \mu_{t-\Delta t^{\mathrm{D}}}^{+\star} = \mu_{\mathrm{ss}}^{+\star}$, $\mu_t^{-\star} = \mu_{t-\Delta t^{\mathrm{D}}}^{-\star} = \mu_{\mathrm{ss}}^{-\star}$. Similarly, suppose there exists $t_{\mathrm{ss}}^{\mathrm{S}}\in\mathcal{T}_{t_0}^{\mathrm{S}}$ such that for all $t'\in\{t_{\mathrm{ss}}^{\mathrm{S}}+\Delta t^{\mathrm{S}},\dots,t_0+T\}$, $\gamma_{t'}^\star = \gamma_{t'-\Delta t^{\mathrm{S}}}^\star = \gamma_{\mathrm{ss}}^\star$ and $\kappa_{t'}^\star = \kappa_{t'-\Delta t^{\mathrm{S}}}^\star = \kappa_{\mathrm{ss}}^\star$. Also assume that neither line-flow nor steady-state generator-capacity constraints are binding, so that $\phi^{+\star} = \phi^{-\star} = \mathbb{0}_L$ and $\mu_{\mathrm{ss}}^{+\star} - \mu_{\mathrm{ss}}^{-\star} = \mathbb{0}_G$. Further, if

$$\pi > \frac{1}{D_{\mathrm{eff}} + R_{\mathrm{eff}}^{-1}}R^{-1}\mathbb{1}_G, \quad (17)$$

where $D_{\mathrm{eff}} = \mathbb{1}_G^{\mathrm{T}}D$ and $R_{\mathrm{eff}}^{-1} = \mathbb{1}_G^{\mathrm{T}}R^{-1}\mathbb{1}_G$, then $\Delta t^{\mathrm{S}} = \Delta t^{\mathrm{D}}$ and $\mathcal{T}_{t_0}^{\mathrm{S}} = \mathcal{T}_{t_0}^{\mathrm{D}}$ must hold.

We refer interested readers to Appendix B for a proof of Proposition 1. The condition in (17) essentially represents the scenario in which all generators contribute sufficiently to AGC, with $\pi_g > R_g^{-1}/(D_{\mathrm{eff}} + R_{\mathrm{eff}}^{-1}) > 0$, $\forall\, g\in\mathcal{G}$. Proposition 1 implies that if $\Delta t^{\mathrm{S}} \neq \Delta t^{\mathrm{D}}$, then under fairly benign operating conditions (i.e., nonbinding inequality constraints and adequate AGC participation from all generators), dynamics-aware LMPs solved from (7) would not reach steady state even if the physical system were to do so.

### B. Dynamical System for LMPs

Considering only dynamics-aware LMPs that *can* reach steady state, we set $\Delta t^{\mathrm{S}} = \Delta t^{\mathrm{D}}$ and use the KKT conditions to derive a dynamical system for the Lagrange multipliers solved from the problem in (7).

**Proposition 2.** Let $\Delta t^{\mathrm{S}} = \Delta t^{\mathrm{D}}$ and $\mathcal{T}_{t_0}^{\mathrm{S}} = \mathcal{T}_{t_0}^{\mathrm{D}}$. Define scaled Lagrange multipliers $\lambda_t'^\star = \lambda_t^\star/\Delta t^{\mathrm{D}}$, $\alpha_t'^\star = \alpha_t^\star/\Delta t^{\mathrm{D}}$, $\beta_t'^\star = \beta_t^\star/\Delta t^{\mathrm{D}}$, $\gamma_t'^\star = \gamma_t^\star/\Delta t^{\mathrm{D}}$, $\mu_t'^{+\star} = \mu_t^{+\star}/\Delta t^{\mathrm{D}}$, $\mu_t'^{-\star} = \mu_t^{-\star}/\Delta t^{\mathrm{D}}$, $\phi'^{+\star} = \phi^{+\star}/\Delta t^{\mathrm{D}}$, and $\phi'^{-\star} = \phi^{-\star}/\Delta t^{\mathrm{D}}$, $t\in\mathcal{T}_{t_0}^{\mathrm{D}}$. Also let $x_t^\star = [\lambda_t'^\star, (\beta_t'^\star)^{\mathrm{T}}, \gamma_t'^\star]^{\mathrm{T}}$ and

$$u_t^{\mu\star} = \frac{\partial C(P_t^{\mathrm{m}\star})}{\partial P_t^{\mathrm{m}\star}} + \mu_t'^{+\star} - \mu_t'^{-\star},\ u^{\phi\star} = \phi'^{+\star} - \phi'^{-\star}. \quad (18)$$

Then, with final condition

$$x_{t_0+T-\Delta t^{\mathrm{D}}}^\star = \begin{bmatrix} -\frac{1}{|\mathcal{T}_{t_0}^{\mathrm{D}}|}\mathbb{1}_G K^{\mathrm{T}}\Psi^{\mathrm{T}}u^{\phi\star} \\ -\tau^{-1}\frac{\partial C(P_{t_0+T}^{\mathrm{m}\star})}{\partial P_{t_0+T}^{\mathrm{m}\star}}\Delta t^{\mathrm{D}} \\ 0 \end{bmatrix}, \quad (19)$$

the optimal trajectory of the scaled Lagrange multipliers is governed by the following discrete-time state-space model:

$$x_{t-\Delta t^{\mathrm{D}}}^\star = Ax_t^\star + B^\mu u_t^{\mu\star} + B^\phi u^{\phi\star}, \quad (20)$$

where matrices $A$, $B^\mu$, and $B^\phi$ are given by

$$A = \Delta t^{\mathrm{D}}\begin{bmatrix} \frac{h}{M_{\mathrm{eff}}} & -\big(\frac{1}{M_{\mathrm{eff}}}R^{-1}\mathbb{1}_G + \frac{1}{\tau_{\mathrm{A}}}\pi\big)^{\mathrm{T}} & \frac{m}{M_{\mathrm{eff}}} - \frac{r}{\tau_{\mathrm{A}}} \\ \tau^{-1}\mathbb{1}_G & \tau^{-1}H & \tau^{-1}\mathbb{1}_G \\ 0 & \frac{1}{\tau_{\mathrm{A}}}\pi^{\mathrm{T}} & \frac{r}{\tau_{\mathrm{A}}} \end{bmatrix},$$

$$B^{\mu} = -\Delta t^{\mathrm{D}} \begin{bmatrix} \mathbb{0}_G^{\mathrm{T}} \\ \tau^{-1} \\ \mathbb{0}_G^{\mathrm{T}} \end{bmatrix}, \; B^{\phi} = \frac{\Delta t^{\mathrm{D}}}{|\mathcal{T}_{t_0}^{\mathrm{D}}|} \begin{bmatrix} \frac{1}{M_{\mathrm{eff}}} D^{\mathrm{T}} K^{\mathrm{T}} \Psi^{\mathrm{T}} \\ -\tau^{-1} K^{\mathrm{T}} \Psi^{\mathrm{T}} \\ \mathbb{0}_L^{\mathrm{T}} \end{bmatrix}, \quad (21)$$

with $M_{\mathrm{eff}} = \mathbb{1}_G^{\mathrm{T}} M$, $h = \frac{M_{\mathrm{eff}}}{\Delta t^{\mathrm{D}}} - D_{\mathrm{eff}}$, $m = h + kb$, $r = \frac{\tau_{\mathrm{A}}}{\Delta t^{\mathrm{D}}} - 1$, and $H = \frac{1}{\Delta t^{\mathrm{D}}} \tau - I_G$. Also, $I_G$ denotes the $G$-dimensional identity matrix.

Proposition 2 represents the outcome of straightforward (although admittedly algebraically intensive) manipulations of the stationarity conditions (25)–(31) and (34) in Appendix A. Thus, for brevity, we refrain from including a proof. Instead, we offer a few observations on the system in (20), in which inputs $u_t^{\mu\star}$ and $u^{\phi\star}$ drive dynamics in state variables $\lambda_t'^{\star}$, $\beta_t'^{\star}$, and $\gamma_t'^{\star}$. It is a backward difference equation, implying the recursion on the Lagrange multipliers runs backward in time from the final condition in (19), in contrast to the recursion for the power system dynamics that run forward in time. Furthermore, entries of $\mu_t'^{+\star}$ ($\mu_t'^{-\star}$) are nonzero only if the upper (lower) mechanical power limits of the corresponding generators are binding, otherwise they are zero. Similarly, entries of $\phi'^{+\star}$ ($\phi'^{-\star}$) are nonzero only if the upper (lower) active-power flow limits of the corresponding lines are binding, otherwise they are zero. Consider the special case where the aforementioned inequality constraints are not binding. Then (20) simplifies as

$$x_{t-\Delta t^{\mathrm{D}}}^{\star} = A x_t^{\star} + B^{\mu} \frac{\partial C(P_t^{\mathrm{m}\star})}{\partial P_t^{\mathrm{m}\star}}, \quad (22)$$

so the dynamics in Lagrange multipliers are (unsurprisingly) driven by the marginal cost of generation in the power system. Since the cost of generation is typically approximated as a quadratic function, the entries in $\frac{\partial C(P_t^{\mathrm{m}\star})}{\partial P_t^{\mathrm{m}\star}}$ would be linear functions of optimal mechanical power at time $t \in \mathcal{T}_{t_0}^{\mathrm{D}}$.

**Example 2** (3-Generator 9-Bus System)**.** In this example, we consider the same system and simulation setup as Example 1 and validate findings in Section IV. Particularly, using the three sets of generator dynamic parameters reported in Table I, we compare LMPs accompanying the optimal solutions of the dynamics-aware and traditional EDs in (7) and (1), respectively. Both versions of the ED are solved in the YALMIP toolbox in MATLAB using GUROBI as the solver [44]. To establish the benchmark, we solve the traditional ED twice, the first with the initial loads and the second with the post-disturbance steady-state loads, thus leading to two sets of LMPs (and two sets of generator set-points). In the dynamics-aware ED, the scheduling horizon is $T = 300\,[\mathrm{sec}]$ (or $5\,[\mathrm{min}]$) starting from $t_0 = 0\,[\mathrm{sec}]$, the time step capturing faster frequency dynamics is set as $\Delta t^{\mathrm{D}} = 0.05\,[\mathrm{sec}]$, and following Proposition 1, we set $\Delta t^{\mathrm{S}} = \Delta t^{\mathrm{D}}$. Here, it is worth mentioning that $\Delta t^{\mathrm{D}}$ can be a smaller value if needed to improve the accuracy of the discrete-time dynamical model, at the expense of greater computational burden to solve (7). In Fig. 2, we plot dynamics-aware LMPs in (12) and superimpose them onto the traditional LMPs in (2). Spatially, all buses have the same LMPs as none of the inequality constraints are binding. Temporally, the dynamics-aware LMPs reflect pricing under different dynamic frequency response scenarios

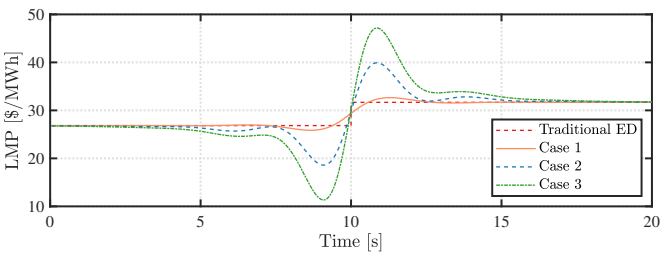


Fig. 2: (Example 2). Comparing LMPs at bus 5 solved from the traditional and dynamics-aware EDs with three different sets of generator parameter values in response to a load increase. Traditional LMPs remain at the same values in all three cases, whereas the dynamics-aware LMPs reflect pricing for differences in dynamic performance observed in Fig. 1.

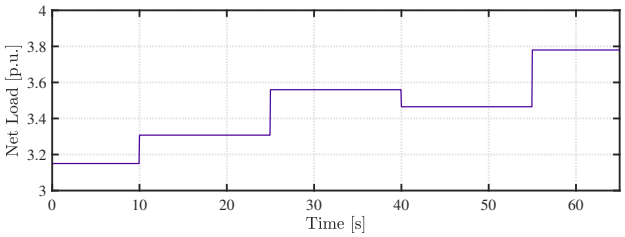


Fig. 3: Total system net-load forecast profile.

shown in Fig. 1b. For more desirable frequency response in case 2 and even more so in case 3, the larger post-disturbance LMPs lead to greater compensation for generators to provide dynamic frequency support. In steady state, the dynamics-aware LMPs converge to the LMPs solved from the traditional ED. However, the traditional LMPs remain constant across the entire post-disturbance transient period and offer the same rate of compensation to generators regardless of their contributions to dynamic performance.

## V. Case Studies

In this section, we present numerical simulations involving the WSCC test system and evaluate the proposed method with respect to system dynamic performance as well as generator costs and profits in comparison to LMPs resulting from the solution of the traditional ED. Furthermore, simulations involving the New England 10-generator 39-bus and the IEEE 50-generator 145-bus test systems [45], [46] demonstrate computational scalability of the proposed dynamics-aware locational marginal pricing approach.

### A. Dynamic Performance

We present additional numerical results involving the WSCC test system using a simulation setup similar to Example 2, but with several notable differences. First, as the benchmark for comparison, we solve the traditional ED only once with initial loads. This represents the business-as-usual real-time electricity markets, in which the traditional ED is typically run every $5\,[\mathrm{min}]$ for a single-snapshot load forecast, and the generator set-points are not updated during the look-ahead interval [10]–[12]. The dynamics-aware ED uses a more granular load forecast involving multiple changes over the scheduling horizon of $T = 300\,[\mathrm{sec}]$ (or $5\,[\mathrm{min}]$). Specifically, as shown in Fig. 3, at $t = 10$ and $25\,[\mathrm{sec}]$, respectively, all

TABLE II: Generator quadratic cost function coefficients in the WSCC test system.

| Generator | $a_g$[\$/(MW$^2$h)] | $b_g$[\$/MWh] | $c_g$[\$/h] |
|---|---|---|---|
| $g = 1$ | 0.1100 | 5 | 0 |
| $g = 2$ | 0.0850 | 1.2 | 0 |
| $g = 3$ | 0.1225 | 1 | 0 |

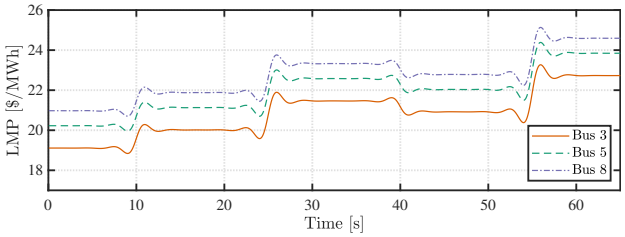


Fig. 4: Dynamics-aware locational marginal prices at (a) bus 3, (b) bus 5, and (c) bus 8, evaluated at the optimal solution of the dynamics-aware ED in (7).

loads are forecasted to increase by 5% and 8%. They then decrease by 3% at $t = 40$ [sec], followed by an increase of 10% at $t = 55$ [sec]. The maximum power flow limit for the line connecting buses 8 and 9 is set to be 0.4 [p.u.], and this constraint becomes binding during the scheduling horizon given the prescribed load forecast. Also, simulations are run with the default dynamical model parameter values from the standard test case, i.e., case 2 in Table I, and with generator cost function coefficients reported in Table II. To extract system dynamic trajectories resulting from the optimal set-points from the traditional ED solution, we apply them as the generator references in a dynamic simulation performed in PSAT [46], where the system frequency is regulated with the AGC described in Section II-B.

*1) Locational Marginal Prices:* We use (12) to evaluate dynamics-aware LMPs at the optimal solution of the ED in (7). The binding line-flow constraint leads to distinct LMPs at different buses, as shown in Fig. 4, with the LMPs at bus 8 being the highest. The constraint applied to the average line flow permits short-term violations of the limit but ensures that it is satisfied in the long term, as shown by the solid trace in Fig. 5 after $t = 55$ [sec]. In contrast, the set-points obtained from the traditional ED violates the line-flow limit for a longer period of time, as shown by the dashed trace in Fig. 5. We also observe in Fig. 4 that within 5 [sec] after each load change, the LMPs converge to steady state, as suggested by Proposition 1. We further validate Proposition 2 by verifying that the LMP trajectories obtained from simulating the discrete-time dynamical system in (20) with the optimal decisions $P_t^{\mathrm{m}\star}$, $\phi^{+\star}$, $\phi^{-\star}$, $\mu_t^{+\star}$, and $\mu_t^{-\star}$ exactly match the traces in Fig. 4.

*2) Frequency Deviations:* As shown in Fig. 6, due to the increase in loads at time $t = 10$ [sec], the system frequency decreases (negative deviation), and updating the generator set-points based on the solution of the dynamics-aware ED leads to lower transient frequency deviations and faster recovery compared to the traditional ED. We observe similar behaviour after all the other load changes as well. The dynamics-aware ED consistently outperforms the traditional ED in terms of dynamic frequency response.

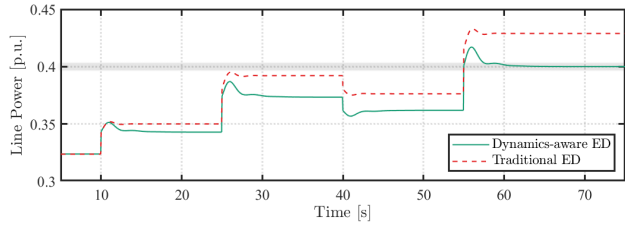


Fig. 5: Time-domain trajectories of active-power flows in the line connecting buses 8 and 9, for which the upper flow limit is 0.4 [p.u.], realized with the dynamics-aware and traditional ED set-points.

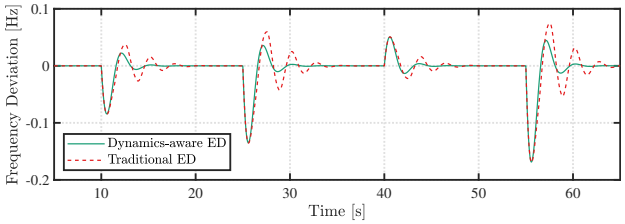


Fig. 6: Time-domain trajectories for system frequency deviations realized with the dynamics-aware and traditional ED set-points.

### *B. Revenues, Costs, and Profits*

We now compare the costs and profits for generators realized by using the LMPs resulting from the proposed dynamics-aware ED and the traditional ED. We use the same simulation setup as in Section V-A, except with different levels of load variations. Starting with the same initial loads, we consider 90%, 100%, 110%, and 120% of the changes forecasted at time $t = 10$, 25, 40, and 55 [sec] in Section V-A. The total revenue is calculated as

$$\sum_{t \in \mathcal{T}_{t_0}^{\mathrm{D}}} \Lambda_t^{\star \mathrm{T}} K P_t^{\star} \Delta t^{\mathrm{D}}, \tag{23}$$

and the total generation cost is calculated as

$$\sum_{t \in \mathcal{T}_{t_0}^{\mathrm{D}}} C\left(P_t^{\mathrm{m}\star}\right) \Delta t^{\mathrm{D}}. \tag{24}$$

Total profit is then obtained by subtracting cost from revenue, where the dynamics-aware LMPs in $\Lambda_t^{\star}$, the generator electrical output $P_t^{\star}$, and the generator mechanical power $P_t^{\mathrm{m}\star}$ are readily available from the optimal solution of the dynamics-aware ED in (7). For comparison, we solve the traditional ED with the initial loads to obtain the optimal generator set-points and the corresponding dynamics-oblivious LMPs in $\Lambda_{\circ}^{\star}$, and ensuing mechanical power trajectories are obtained from a PSAT simulation with the AGC regulating system frequency. Revenue in the dynamics-oblivious case is calculated using (23) with $\Lambda_t^{\star} = \Lambda_{\circ}^{\star}, \forall\, t \in \mathcal{T}_{t_0}^{\mathrm{D}}$. In Fig. 7, for each load forecast scenario, we plot the total cost and profit, which sum to the total revenue. We observe that the dynamics-aware LMPs yield greater revenues and profits for generators compared to their traditional static counterparts, while the two methods lead to nearly identical costs. Although the total revenue in (23) is calculated as a sum over each $\Delta t^{\mathrm{D}}$ interval, practical considerations in market settlement periods may impose summation over longer time intervals using sampled values of LMPs over the scheduling horizon.

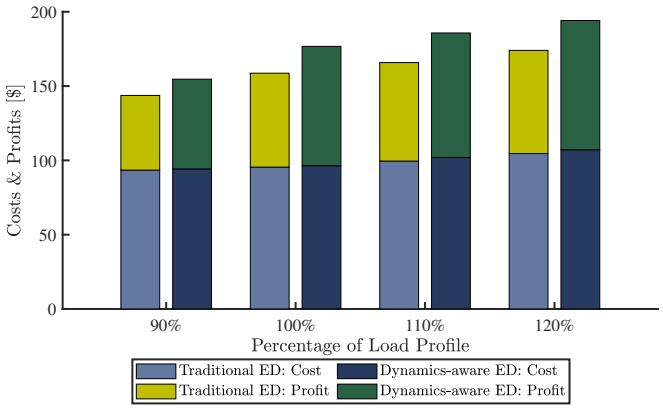


Fig. 7: Total costs and profits of generators resulting from traditional and dynamics-aware EDs for different levels of changes in forecasted loads.

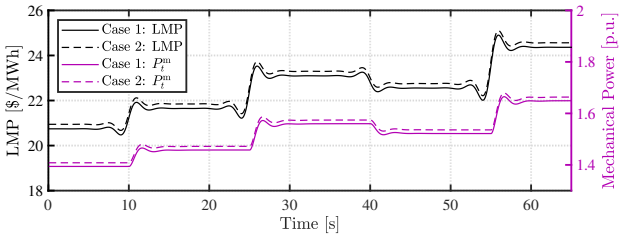


Fig. 8: Impact of setting generator inertia constants to (case 1) $M_2 = 6.4\,[\mathrm{sec}]$ and $M_3 = 3.01\,[\mathrm{sec}]$ and (case 2) $M_2 = 1\,[\mathrm{sec}]$ and $M_3 = 8.41\,[\mathrm{sec}]$ on dynamic trajectories of the dynamics-aware LMP at the bus connected to generator 2 and of the turbine mechanical power of generator 2.

### C. Inverter-based Sources

We examine the impact of inverter-based sources governed by virtual synchronous generator controllers on dynamics-aware LMPs. Exploiting the ability for such controllers to set their inertia constants, we ascribe two sets of inertia constants that add up to the same total system inertia of $33.05\,[\mathrm{sec}]$. Case 1 uses the default setting of $M_1 = 23.64\,[\mathrm{sec}]$, $M_2 = 6.4\,[\mathrm{sec}]$, and $M_3 = 3.01\,[\mathrm{sec}]$, while case 2 uses $M_1 = 23.64\,[\mathrm{sec}]$, $M_2 = 1\,[\mathrm{sec}]$, and $M_3 = 8.41\,[\mathrm{sec}]$. We solve the dynamics-aware ED and, in Fig. 8, plot the dynamic trajectories of the turbine mechanical powers (right-hand $y$-axis) and the dynamics-aware LMPs (left-hand $y$-axis). Going from case 1 to case 2, the inertia constant of generator 2 decreases, leading to faster dynamics in response to net-load disturbances. Accordingly, the LMP at the bus connected to generator 2 is greater in case 2 than in case 1. The same trend is observed for generator 3 with greater LMPs associated with smaller inertia constant.

### D. Computational Scalability

The proposed dynamics-aware ED problem is modelled in the YALMIP toolbox in MATLAB and solved using GUROBI on a desktop computer with a $3.6\,[\mathrm{GHz}]$ i7 processor and $32\,[\mathrm{GB}]$ RAM. We solve the proposed dynamics-aware ED for the WSCC, New England, and IEEE 145-bus test systems and report the computation times for scheduling horizons of 100, 200, and 300, and $600\,[\mathrm{sec}]$ in Table III. The reported times include that incurred by the YALMIP compilation and for solving the optimization using GUROBI. Loads are

TABLE III: Computation times [sec] to solve dynamics-aware ED for three standard dynamic test systems over various scheduling horizons.

| Scheduling Horizon [sec] | 100 | 200 | 300 | 600 |
|---|---|---|---|---|
| WSCC (3 generators) | 1.052 | 2.636 | 5.491 | 11.810 |
| New England (10 generators) | 2.189 | 4.203 | 8.427 | 19.974 |
| IEEE 145-bus (50 generators) | 8.906 | 18.169 | 38.035 | 61.721 |

forecasted to change every $15\,[\mathrm{sec}]$ with a randomly selected value between $-5\%$ and $+5\%$. Although the computation time increases for a larger test system, it remains acceptable compared to the scheduling horizons considered. A possible way to improve computational performance is to synthesize discrete-time dynamics in (7b)–(7d) via a method that may afford larger discretization intervals without sacrificing model accuracy, as discussed in Remark 1. Another possibility is to apply dimensionality reduction techniques, i.e., treating decision variables as continuous-time trajectories that cover the entire scheduling horizon and projecting them onto suitable function spaces of desired degrees, such as the function space spanned by Bernstein polynomials [28]. Finally, further reductions in computational burden may be possible via the use of advanced optimization solvers and distributed algorithms.

## VI. Concluding Remarks

In this paper, we presented a dynamics-aware locational marginal pricing scheme that incorporates power system frequency dynamics, including those arising from generators and an industry-standard AGC, as constraints. The dynamics-aware LMPs reflect the effects of system frequency transients after disturbances in load or generation. We provide analysis to describe the dynamic and steady-state behaviours of the dynamics-aware LMPs. Numerical results validate the analytical findings and confirm the benefits of the proposed dynamics-aware LMPs in providing broader revenue opportunities for generators prior to reaching steady state. Future work will address forecast uncertainties through coordinated dynamics- and risk-aware LMPs of energy and reserve capacity, where performance may be guaranteed in a probabilistic manner via chance constraints. Further compelling directions for future work include incorporating frequency dynamics into security-constrained economic dispatch and the optimal power flow problem with nonlinear power flow constraints. Also of interest, especially in these problems of greater complexity, are improvements in computation time by exploring contemporary optimization solution algorithms.

## Appendix

### A. Optimality Conditions of (7)

In addition to (10)–(11), the optimal solution of the problem in (7) also satisfies the following stationarity conditions:

$$0 = \frac{\partial \mathcal{L}^\star}{\partial \Delta\omega_t^\star} = D^{\mathrm{T}}\alpha_t^\star - M^{\mathrm{T}}\Big(\frac{\alpha_t^\star - \alpha_{t-\Delta t^{\mathrm{D}}}^\star}{\Delta t^{\mathrm{D}}}\Big) + \mathbb{1}_G^{\mathrm{T}} R^{-1}\beta_t^\star - \mathcal{O}_t k b \gamma_{t'}^\star,\ t' \in \mathcal{T}_{t_0}^{\mathrm{S}} \setminus \{t_0, t_0+T\}, \quad t \in \{t', \ldots, t' + \Delta t^{\mathrm{S}} - \Delta t^{\mathrm{D}}\}, \tag{25}$$

$$\mathbb{0}_G = \frac{\partial \mathcal{L}^\star}{\partial P_t^{\mathrm{m}\star}} = \frac{\partial C(P_t^{\mathrm{m}\star})}{\partial P_t^{\mathrm{m}\star}}\Delta t^{\mathrm{D}} - \alpha_t^\star + \beta_t^\star + \mu_t^{+\star} - \mu_t^{-\star}$$

$$- \tau\Big(\frac{\beta^\star_t - \beta^\star_{t-\Delta t^{\mathrm{D}}}}{\Delta t^{\mathrm{D}}}\Big),\ t \in \mathcal{T}^{\mathrm{D}}_{t_0} \setminus \{t_0, t_0+T\}, \tag{26}$$

$$\mathbb{0}_G = \frac{\partial \mathcal{L}^\star}{\partial P^\star_t} = -\mathbb{1}_G \lambda^\star_t + \alpha^\star_t - K^{\mathrm{T}} \rho^\star_t - \mathbb{1}_G \mathcal{O}_t \gamma^\star_{t'},$$
$$t' \in \mathcal{T}^{\mathrm{S}}_{t_0} \setminus \{t_0+T\},\ t \in \{t', \ldots, t' + \Delta t^{\mathrm{S}} - \Delta t^{\mathrm{D}}\}, \tag{27}$$

$$\mathbb{0}_G = \frac{\partial \mathcal{L}^\star}{\partial P^{\mathrm{r}\star}_{t'}} = \kappa^\star_{t'} - \sum_{t=t'}^{t'+\Delta t^{\mathrm{S}}-\Delta t^{\mathrm{D}}} \beta^\star_t,\ t' \in \mathcal{T}^{\mathrm{S}}_{t_0} \setminus \{t_0+T\}, \tag{28}$$

$$0 = \frac{\partial \mathcal{L}^\star}{\partial \xi^\star_{t'}} = -\pi^{\mathrm{T}} \kappa^\star_{t'} - \tau_{\mathrm{A}}\Big(\frac{\gamma^\star_{t'} - \gamma^\star_{t'-\Delta t^{\mathrm{S}}}}{\Delta t^{\mathrm{S}}}\Big) + \gamma^\star_{t'},$$
$$t' \in \mathcal{T}^{\mathrm{S}}_{t_0} \setminus \{t_0, t_0+T\}, \tag{29}$$

$$0 = \frac{\partial \mathcal{L}^\star}{\partial \Delta\omega^\star_{t_0+T}} = \frac{1}{\Delta t^{\mathrm{D}}} M^{\mathrm{T}} \alpha^\star_{t_0+T-\Delta t^{\mathrm{D}}}, \tag{30}$$

$$\mathbb{0}_G = \frac{\partial \mathcal{L}^\star}{\partial P^{\mathrm{m}\star}_{t_0+T}} = \frac{\partial C(P^{\mathrm{m}\star}_{t_0+T})}{\partial P^{\mathrm{m}\star}_{t_0+T}} \Delta t^{\mathrm{D}} + \frac{1}{\Delta t^{\mathrm{D}}} \tau \beta^\star_{t_0+T-\Delta t^{\mathrm{D}}}, \tag{31}$$

$$\mathbb{0}_G = \frac{\partial \mathcal{L}^\star}{\partial P^\star_{t_0+T}} = -\mathbb{1}_G \lambda^\star_{t_0+T} - K^{\mathrm{T}} \rho^\star_{t_0+T}, \tag{32}$$

$$\mathbb{0}_G = \frac{\partial \mathcal{L}^\star}{\partial P^{\mathrm{r}\star}_{t_0+T}} = \kappa^\star_{t_0+T}, \tag{33}$$

$$0 = \frac{\partial \mathcal{L}^\star}{\partial \xi^\star_{t_0+T}} = \frac{\tau_{\mathrm{A}}}{\Delta t^{\mathrm{S}}} \gamma^\star_{t_0+T-\Delta t^{\mathrm{S}}} - \pi^{\mathrm{T}} \kappa^\star_{t_0+T}, \tag{34}$$

where $\mathcal{O}_t = 1$ if $t \in \mathcal{T}^{\mathrm{S}}_{t_0}$ and $\mathcal{O}_t = 0$ otherwise. We can further substitute (33) into (34) to get

$$0 = \frac{\partial \mathcal{L}^\star}{\partial \xi^\star_{t_0+T}} = \frac{\tau_{\mathrm{A}}}{\Delta t^{\mathrm{S}}} \gamma^\star_{t_0+T-\Delta t^{\mathrm{S}}}. \tag{35}$$

The optimal solution of the problem in (7) further satisfies complementary slackness conditions, given by the following:

$$\mu^{-\star}_{g,t}(\underline{P}_g - P^{\mathrm{m}\star}_{g,t}) = 0,\ \mu^{-\star}_{g,t} \geq 0,\ g \in \mathcal{G},\ t \in \mathcal{T}^{\mathrm{D}}_{t_0}, \tag{36}$$

$$\mu^{+\star}_{g,t}(P^{\mathrm{m}\star}_{g,t} - \overline{P}_g) = 0,\ \mu^{+\star}_{g,t} \geq 0,\ g \in \mathcal{G},\ t \in \mathcal{T}^{\mathrm{D}}_{t_0}, \tag{37}$$

$$\phi^{-\star}_\ell \Big(\underline{F}_\ell - \frac{1}{|\mathcal{T}^{\mathrm{D}}_{t_0}|} \sum_{t \in \mathcal{T}^{\mathrm{D}}_{t_0}} \Psi_\ell P^{\mathrm{inj}\star}_t\Big) = 0,\ \phi^{-\star}_\ell \geq 0,\ \ell \in \mathcal{L}, \tag{38}$$

$$\phi^{+\star}_\ell \Big(\frac{1}{|\mathcal{T}^{\mathrm{D}}_{t_0}|} \sum_{t \in \mathcal{T}^{\mathrm{D}}_{t_0}} \Psi_\ell P^{\mathrm{inj}\star}_t - \overline{F}_\ell\Big) = 0,\ \phi^{+\star}_\ell \geq 0,\ \ell \in \mathcal{L}, \tag{39}$$

where $\Psi_\ell$ represents row $\ell$ of the matrix $\Psi$.

### *B. Proof of Proposition 1*

We first recognize from (11) that

$$\rho^\star_t = -\frac{1}{|\mathcal{T}^{\mathrm{D}}_{t_0}|} \Psi^{\mathrm{T}}(\phi^{+\star} - \phi^{-\star}) =: \rho^\star_{\mathrm{ss}},\ \forall\, t \in \mathcal{T}^{\mathrm{D}}_{t_0}. \tag{40}$$

We now proceed via proof by contradiction and suppose that $\Delta t^{\mathrm{S}} \neq \Delta t^{\mathrm{D}}$ (so $\mathcal{T}^{\mathrm{S}}_{t_0} \neq \mathcal{T}^{\mathrm{D}}_{t_0}$). In steady state, the optimality condition in (27) becomes

$$\mathbb{0}_G = -\mathbb{1}_G \lambda^\star_{\mathrm{ss}} + \alpha^\star_{\mathrm{ss}} - K^{\mathrm{T}} \rho^\star_{\mathrm{ss}} - \mathbb{1}_G \mathcal{O}_t \gamma^\star_{\mathrm{ss}},\ t \in \mathcal{T}^{\mathrm{D}}_{t_0}. \tag{41}$$

By writing (41) separately for $t \notin \mathcal{T}^{\mathrm{S}}_{t_0}$ and $t \in \mathcal{T}^{\mathrm{S}}_{t_0}$, we get

$$\mathbb{0}_G = -\mathbb{1}_G \lambda^\star_{\mathrm{ss}} + \alpha^\star_{\mathrm{ss}} - K^{\mathrm{T}} \rho^\star_{\mathrm{ss}}, \qquad \text{if } t \notin \mathcal{T}^{\mathrm{S}}_{t_0}, \tag{42}$$

$$\mathbb{0}_G = -\mathbb{1}_G \lambda^\star_{\mathrm{ss}} + \alpha^\star_{\mathrm{ss}} - K^{\mathrm{T}} \rho^\star_{\mathrm{ss}} - \mathbb{1}_G \gamma^\star_{\mathrm{ss}}, \quad \text{if } t \in \mathcal{T}^{\mathrm{S}}_{t_0}, \tag{43}$$

implying that $\gamma^\star_{\mathrm{ss}} = 0$ for both statements to hold in steady state. Thus, (41) simplifies as $\alpha^\star_{\mathrm{ss}} = \mathbb{1}_G \lambda^\star_{\mathrm{ss}} + K^{\mathrm{T}} \rho^\star_{\mathrm{ss}}$, and we will find the following scaling of this expression useful:

$$\mathbb{1}^{\mathrm{T}}_G R^{-1} \alpha^\star_{\mathrm{ss}} = R^{-1}_{\mathrm{eff}} \lambda^\star_{\mathrm{ss}} + \mathbb{1}^{\mathrm{T}}_G R^{-1} K^{\mathrm{T}} \rho^\star_{\mathrm{ss}}, \tag{44}$$

$$D^{\mathrm{T}} \alpha^\star_{\mathrm{ss}} = D_{\mathrm{eff}} \lambda^\star_{\mathrm{ss}} + D^{\mathrm{T}} K^{\mathrm{T}} \rho^\star_{\mathrm{ss}}, \tag{45}$$

$$\pi^{\mathrm{T}} \alpha^\star_{\mathrm{ss}} = \lambda^\star_{\mathrm{ss}} + \pi^{\mathrm{T}} K^{\mathrm{T}} \rho^\star_{\mathrm{ss}}, \tag{46}$$

where we have made use of the fact that $\pi^{\mathrm{T}} \mathbb{1}_G = \mathbb{1}^{\mathrm{T}}_G \pi = 1$ in (46). Next we evaluate (26) in steady state as follows:

$$\alpha^\star_{\mathrm{ss}} = \frac{\partial C(P^{\mathrm{m}\star}_{\mathrm{ss}})}{\partial P^{\mathrm{m}\star}_{\mathrm{ss}}} \Delta t^{\mathrm{D}} + \beta^\star_{\mathrm{ss}} + \mu^{+\star}_{\mathrm{ss}} - \mu^{-\star}_{\mathrm{ss}}. \tag{47}$$

We will find the following scaling of (47) useful:

$$\mathbb{1}^{\mathrm{T}}_G R^{-1} \alpha^\star_{\mathrm{ss}} = \mathbb{1}^{\mathrm{T}}_G R^{-1}\Big(\frac{\partial C(P^{\mathrm{m}\star}_{\mathrm{ss}})}{\partial P^{\mathrm{m}\star}_{\mathrm{ss}}} \Delta t^{\mathrm{D}} + \mu^{+\star}_{\mathrm{ss}} - \mu^{-\star}_{\mathrm{ss}}\Big) + \mathbb{1}^{\mathrm{T}}_G R^{-1} \beta^\star_{\mathrm{ss}}, \tag{48}$$

$$\pi^{\mathrm{T}} \alpha^\star_{\mathrm{ss}} = \pi^{\mathrm{T}}\Big(\frac{\partial C(P^{\mathrm{m}\star}_{\mathrm{ss}})}{\partial P^{\mathrm{m}\star}_{\mathrm{ss}}} \Delta t^{\mathrm{D}} + \mu^{+\star}_{\mathrm{ss}} - \mu^{-\star}_{\mathrm{ss}}\Big) + \pi^{\mathrm{T}} \beta^\star_{\mathrm{ss}}. \tag{49}$$

Equating (44) and (48) and rearranging the resultant, we get

$$\mathbb{1}^{\mathrm{T}}_G R^{-1} \beta^\star_{\mathrm{ss}} = R^{-1}_{\mathrm{eff}} \lambda^\star_{\mathrm{ss}} + \mathbb{1}^{\mathrm{T}}_G R^{-1} K^{\mathrm{T}} \rho^\star_{\mathrm{ss}} - \mathbb{1}^{\mathrm{T}}_G R^{-1}\Big(\frac{\partial C(P^{\mathrm{m}\star}_{\mathrm{ss}})}{\partial P^{\mathrm{m}\star}_{\mathrm{ss}}} \Delta t^{\mathrm{D}} + \mu^{+\star}_{\mathrm{ss}} - \mu^{-\star}_{\mathrm{ss}}\Big). \tag{50}$$

Shift focus now to express (25) in steady state, while recognizing that $\gamma^\star_{\mathrm{ss}} = 0$, as follows:

$$0 = D^{\mathrm{T}} \alpha^\star_{\mathrm{ss}} + \mathbb{1}^{\mathrm{T}}_G R^{-1} \beta^\star_{\mathrm{ss}}. \tag{51}$$

Further substitute (45) and (50) into (51) and rearrange the resultant to get

$$\lambda^\star_{\mathrm{ss}} = \frac{1}{D_{\mathrm{eff}} + R^{-1}_{\mathrm{eff}}}\Big( - (\mathbb{1}^{\mathrm{T}}_G R^{-1} + D^{\mathrm{T}}) K^{\mathrm{T}} \rho^\star_{\mathrm{ss}} + \mathbb{1}^{\mathrm{T}}_G R^{-1}\Big(\frac{\partial C(P^{\mathrm{m}\star}_{\mathrm{ss}})}{\partial P^{\mathrm{m}\star}_{\mathrm{ss}}} \Delta t^{\mathrm{D}} + \mu^{+\star}_{\mathrm{ss}} - \mu^{-\star}_{\mathrm{ss}}\Big)\Big). \tag{52}$$

Next, we examine the optimality condition in (29) in steady state, as follows:

$$0 = -\pi^{\mathrm{T}} \kappa^\star_{\mathrm{ss}} + \gamma^\star_{\mathrm{ss}} = -\pi^{\mathrm{T}} \kappa^\star_{\mathrm{ss}}, \tag{53}$$

where the second equality holds by recognizing that $\gamma^\star_{\mathrm{ss}} = 0$. Now we express the optimality condition in (28) in steady state and pre-multiply the resultant by $\pi^{\mathrm{T}}$ to get

$$0 = \pi^{\mathrm{T}} \kappa^\star_{\mathrm{ss}} - \sum_{t=t'}^{t'+\Delta t^{\mathrm{S}}-\Delta t^{\mathrm{D}}} \pi^{\mathrm{T}} \beta^\star_{\mathrm{ss}} = \pi^{\mathrm{T}} \kappa^\star_{\mathrm{ss}} - \frac{|\mathcal{T}^{\mathrm{D}}_{t_0}| - 1}{|\mathcal{T}^{\mathrm{S}}_{t_0}| - 1} \pi^{\mathrm{T}} \beta^\star_{\mathrm{ss}}. \tag{54}$$

Substitution of (53) into (54) yields $\pi^{\mathrm{T}} \beta^\star_{\mathrm{ss}} = 0$. With this in mind, we equate (46) and (49) to get

$$\lambda^\star_{\mathrm{ss}} = -\pi^{\mathrm{T}} K^{\mathrm{T}} \rho^\star_{\mathrm{ss}} + \pi^{\mathrm{T}}\Big(\frac{\partial C(P^{\mathrm{m}\star}_{\mathrm{ss}})}{\partial P^{\mathrm{m}\star}_{\mathrm{ss}}} \Delta t^{\mathrm{D}} + \mu^{+\star}_{\mathrm{ss}} - \mu^{-\star}_{\mathrm{ss}}\Big). \tag{55}$$

Bearing in mind (40), we take the difference between (55) and (52) to get

$$0 = \frac{1}{|\mathcal{T}^{\mathrm{D}}_{t_0}|}\Big(\pi - \frac{1}{D_{\mathrm{eff}} + R^{-1}_{\mathrm{eff}}}(R^{-1}\mathbb{1}_G + D)\Big)^{\mathrm{T}} \cdot K^{\mathrm{T}} \Psi^{\mathrm{T}}(\phi^{+\star} - \phi^{-\star}) + \Big(\pi - \frac{1}{D_{\mathrm{eff}} + R^{-1}_{\mathrm{eff}}} R^{-1}\mathbb{1}_G\Big)^{\mathrm{T}}$$

$$\cdot \Big( \frac{\partial C(P_{\rm ss}^{\rm m\star})}{\partial P_{\rm ss}^{\rm m\star}} \Delta t^{\rm D} + \mu_{\rm ss}^{+\star} - \mu_{\rm ss}^{-\star} \Big). \tag{56}$$

Under the additional assumptions that $\phi^{+\star} = \phi^{-\star} = \mathbb{0}_L$ and $\mu_{\rm ss}^{+\star} = \mu_{\rm ss}^{-\star} = \mathbb{0}_G$, (56) simplifies as

$$0 = \Big( \pi - \frac{1}{D_{\rm eff} + R_{\rm eff}^{-1}} R^{-1} \mathbb{1}_G \Big)^{\rm T} \frac{\partial C(P_{\rm ss}^{\rm m\star})}{\partial P_{\rm ss}^{\rm m\star}} \Delta t^{\rm D}. \tag{57}$$

Now, if the entries in the first vector of the inner product above are all positive valued as implied by the condition in (17), the second vector therein must contain a mix of positive- and negative-valued entries or all entries must be identically zero. Having *some* negative-valued entries contradicts the convexity of cost functions, and having *all* zero-valued entries implies that cost functions are independent of generated power which is not reasonable. Thus, the assumption at the beginning of the proof is invalid, and indeed, $\Delta t^{\rm S} = \Delta t^{\rm D}$ must hold if there exist steady-state Lagrange multipliers.

## REFERENCES


[1] P. Denholm, T. Mai, R. W. Kenyon, B. Kroposki, and M. O'malley, "Inertia and the power grid: A guide without the spin," National Renewable Energy Laboratory, Golden, CO (United States), Tech. Rep., May. 2020.

[2] L. Bird, M. Milligan, and D. Lew, "Integrating variable renewable energy: Challenges and solutions," National Renewable Energy Laboratory, Golden, CO (United States), Tech. Rep., Sep. 2013.

[3] T. Mai, R. Wiser, G. Barbose, L. Bird, J. Heeter, D. Keyser, V. Krishnan, J. Macknick, and D. Millstein, "A prospective analysis of the costs, benefits, and impacts of us renewable portfolio standards," National Renewable Energy Laboratory, Golden, CO (United States), Tech. Rep., Dec. 2016.

[4] U. Tamrakar, D. Shrestha, M. Maharjan, B. P. Bhattarai, T. M. Hansen, and R. Tonkoski, "Virtual inertia: Current trends and future directions," *Appl. Sci.*, vol. 7, no. 7, p. 654, 2017.

[5] E. Ela, C. Wang, S. Moorty, K. Ragsdale, J. O'Sullivan, M. Rothleder, and B. Hobbs, "Electricity markets and renewables: a survey of potential design changes and their consequences," *IEEE Power and Energy Mag.*, vol. 15, no. 6, pp. 70–82, Oct. 2017.

[6] "Business practice manual for market operations, version 65," California ISO, 2020.

[7] "Business practices manual: Energy and operating reserve markets," Midcontinent ISO, 2016.

[8] J. D. Glover, T. J. Overbye, M. S. Sarma, and A. B. Birchfield, *Power System Analysis and Design*. Cengage Learning, 2023.

[9] D. S. Kirschen and G. Strbac, *Fundamentals of power system economics*. John Wiley & Sons, 2018.

[10] A. L. Ott, "Experience with PJM market operation, system design, and implementation," *IEEE Trans. Power Syst.*, vol. 18, no. 2, pp. 528–534, May 2003.

[11] E. Litvinov, T. Zheng, G. Rosenwald, and P. Shamsollahi, "Marginal loss modeling in LMP calculation," *IEEE Trans. Power Syst.*, vol. 19, no. 2, pp. 880–888, May 2004.

[12] E. Litvinov, "Power system & LMP fundamentals," EE/Econ 458, Iowa State University, Ames, IA, 2009. [Online]. Available: http://www2.econ.iastate.edu/classes/econ458/tesfatsion/lmp.AdvancedWPM.ELitvinovWEM301.pdf

[13] D. Obradović, M. Dijokas, G. S. Misyris, T. Weckesser, and T. Van Cutsem, "Frequency dynamics of the Northern European AC/DC power system: A look-ahead study," *IEEE Trans. on Power Syst.*, vol. 37, no. 6, pp. 4661–4672, Jul. 2022.

[14] B. K. Poolla, S. Bolognani, N. Li, and F. Dörfler, "A market mechanism for virtual inertia," *IEEE Trans. Smart Grid*, vol. 11, no. 4, pp. 3570–3579, Jan. 2020.

[15] L. Badesa, F. Teng, and G. Strbac, "Pricing inertia and frequency response with diverse dynamics in a mixed-integer second-order cone programming formulation," *Appl. Energy*, vol. 260, pp. 1–11, Feb. 2020.

[16] M. Paturet, U. Markovic, S. Delikaraoglou, E. Vrettos, P. Aristidou, and G. Hug, "Economic valuation and pricing of inertia in inverter-dominated power systems," *arXiv preprint arXiv:2005.11029*, May. 2020.

[17] E. Ela, V. Gevorgian, A. Tuohy, B. Kirby, M. Milligan, and M. O'Malley, "Market designs for the primary frequency response ancillary service–part I: Motivation and design," *IEEE Trans. Power Syst.*, vol. 29, no. 1, pp. 421–431, Jun. 2013.

[18] Z. Liang, R. Mieth, and Y. Dvorkin, "Inertia pricing in stochastic electricity markets," 2021. [Online]. Available: https://arxiv.org/abs/2107.04101v1

[19] R. Khatami, A. Al-Digs, and Y. C. Chen, "Frequency dynamics-aware real-time marginal pricing of electricity," *Electr. Power Syst. Res.*, vol. 212, p. 108429, Nov. 2022.

[20] Q. Wang, G. Zhang, J. D. McCalley, T. Zheng, and E. Litvinov, "Risk-based locational marginal pricing and congestion management," *IEEE Trans. Power Syst.*, vol. 29, no. 5, pp. 2518–2528, Feb. 2014.

[21] X. Fang, B.-M. Hodge, E. Du, C. Kang, and F. Li, "Introducing uncertainty components in locational marginal prices for pricing wind power and load uncertainties," *IEEE Trans. Power Syst.*, vol. 34, no. 3, pp. 2013–2024, Jan. 2019.

[22] D. A. Schiro, T. Zheng, F. Zhao, and E. Litvinov, "Convex hull pricing in electricity markets: Formulation, analysis, and implementation challenges," *IEEE Trans. Power Syst.*, vol. 31, no. 5, pp. 4068–4075, Oct. 2015.

[23] B. Hua and R. Baldick, "A convex primal formulation for convex hull pricing," *IEEE Trans. Power Syst.*, vol. 32, no. 5, pp. 3814–3823, Dec. 2016.

[24] B. Hua, D. A. Schiro, T. Zheng, R. Baldick, and E. Litvinov, "Pricing in multi-interval real-time markets," *IEEE Trans. Power Syst.*, vol. 34, no. 4, pp. 2696–2705, Jan. 2019.

[25] R. Khatami and M. Parvania, "Continuous-time locational marginal price of electricity," *IEEE Access*, vol. 7, pp. 129 480–129 493, Sep. 2019.

[26] Z. Tan, T. Cheng, Y. Liu, and H. Zhong, "Extensions of the locational marginal price theory in evolving power systems: A review," *IET Generat., Transmission, Distribut.*, vol. 16, no. 7, pp. 1277–1291, Apr. 2022.

[27] G. Zhang, J. McCalley, and Q. Wang, "An AGC dynamics-constrained economic dispatch model," *IEEE Trans. Power Syst.*, vol. 34, no. 5, pp. 3931–3940, Apr. 2019.

[28] R. Khatami, M. Parvania, C. Chen, S. S. Guggilam, and S. V. Dhople, "Dynamics-aware continuous-time economic dispatch: A solution for optimal frequency regulation." in *Proc. Hawaii Int. Conf. Syst. Sci.*, Jan. 2020, pp. 3186–3195.

[29] V. Trovato, "System scheduling with optimal time-varying delivery intervals for frequency response," *IEEE Trans. on Power Syst.*, vol. 37, no. 6, pp. 4270–4285, Feb. 2022.

[30] A. J. Wood, B. F. Wollenberg, and G. B. Sheblé, *Power generation, operation, and control, 3rd Edition*. John Wiley & Sons, 2013.

[31] S. V. Dhople, Y. C. Chen, A. Al-Digs, and A. D. Domínguez-García, "Reexamining the distributed slack bus," *IEEE Trans. Power Syst.*, vol. 35, no. 6, pp. 4870–4879, Nov. 2020.

[32] F. P. DeMello, R. J. Mills, and W. F. B'Rells, "Automatic generation control part II-digital control techniques," *IEEE Trans. Power App. Syst.*, vol. PAS-92, no. 2, pp. 716–724, Mar. 1973.

[33] W. B. Gish, "Automatic generation control - notes and observations," Electric Power Branch, Division of Research, Engineering and Research Center, Tech. Rep. REC-ERC-78-6, Oct. 1978.

[34] M. D. Ilić and Q. Liu, *Toward Sensing, Communications and Control Architectures for Frequency Regulation in Systems with Highly Variable Resources*. New York, NY: Springer New York, 2012, pp. 3–33.

[35] P. W. Sauer and M. A. Pai, *Power System Dynamics and Stability*. Upper Saddle River, NJ: Prentice-Hall, Inc., 1998.

[36] A. D. Domínguez-García, "Models for impact assessment of wind-based power generation on frequency control," in *Control and Optimization Methods for Electric Smart Grids*. Springer, 2012, pp. 149–165.

[37] Q.-C. Zhong and G. Weiss, "Synchronverters: Inverters that mimic synchronous generators," *IEEE Trans. Ind. Electron*, vol. 58, no. 4, pp. 1259–1267, Apr. 2010.

[38] S. Dong and Y. C. Chen, "Adjusting synchronverter dynamic response speed via damping correction loop," *IEEE Trans. Energy Convers.*, vol. 32, no. 2, pp. 608–619, Dec. 2017.

[39] J. A. Mueller, M. Rasheduzzaman, and J. W. Kimball, "A model modification process for grid-connected inverters used in islanded microgrids," *IEEE Trans. Energy Convers.*, vol. 31, no. 1, pp. 240–250, Mar. 2016.

[40] A. R. Al-Roomi, "Power Flow Test Systems Repository," Halifax, Nova Scotia, Canada, 2015. [Online]. Available: https://al-roomi.org/power-flow

[41] M. Garcia, R. Baldick, and F. Wilches Bernal, "Pricing frequency response market products for inverter-based resources." Sandia National Laboratory, Albuquerque, NM (United States), Tech. Rep., 2020.

[42] J. Hetzer, C. Y. David, and K. Bhattarai, "An economic dispatch model incorporating wind power," *IEEE Trans. Energy Convers.*, vol. 23, no. 2, pp. 603–611, Apr. 2008.
[43] W. Li, "Transparency and explainability in financial data science," Norwegian University of Science and Technology, Dec. 2021.
[44] Gurobi Optimization, LLC, "Gurobi Optimizer Reference Manual," 2023. [Online]. Available: https://www.gurobi.com
[45] I. Hiskens, "IEEE PES task force on benchmark systems for stability controls," *Technical report*, 2013.
[46] F. Milano, "An open source power system analysis toolbox," *IEEE Trans. Power Syst.*, vol. 20, no. 3, pp. 1199–1206, Aug. 2005.

**Bo Chen (S'20)** received the B.S. degree in electrical engineering from Sichuan University, Chengdu, China, in 2015, and the M.A.Sc. degree in Electrical and Computer Engineering from The University of British Columbia, Vancouver, BC, Canada in 2019, where he is currently working toward the Ph.D. degree. His research interests include power system operation and electricity markets.

**Roohallah Khatami** received his B.Sc., M.S., and Ph.D. degrees respectively from Iran University of Science and Technology, Tehran, Iran, in 2007, Amirkabir University of Technology, Tehran, Iran, in 2013, and the University of Utah, Salt Lake City, UT, USA, in 2019, all in electrical engineering. He was a Postdoctoral Research Associate with the Department of Industrial & Systems Engineering, Texas A&M University, College Station, TX, USA, a Postdoctoral Research Fellow with the Department of Electrical and Computer Engineering, the University of British Columbia, Vancouver, BC, Canada, and he is currently an Assistant Professor in the School of Electrical, Computer, and Biomedical Engineering at Southern Illinois University at Carbondale, IL, USA. His research interests include power systems operation and electricity markets.

**Abdullah Al-Digs (S'14–M'21)** received the B.A.Sc. and Ph.D. degrees in electrical engineering from The University of British Columbia, Vancouver, BC, Canada, in 2015 and 2021, respectively. He is currently a Project Lead and Senior Power System Studies Consultant at PSC North America. He is an Adjunct Professor in the Department of Electrical and Computer Engineering at The University of British Columbia. His research interests include power system analysis, operation, monitoring, and control.

**Yu Christine Chen (S'10–M'15)** received the B.A.Sc. degree in engineering science from the University of Toronto, Toronto, ON, Canada, in 2009, and the M.S. and Ph.D. degrees in electrical engineering from the University of Illinois at Urbana-Champaign, Urbana, IL, USA, in 2011 and 2014, respectively. She is currently an Associate Professor in the Department of Electrical and Computer Engineering, The University of British Columbia, Vancouver, BC, Canada, where she is affiliated with the Electric Power and Energy Systems Group. Her research interests include power system analysis, operation, and control. She is a recipient of a Best Paper Award from the *IEEE Transactions on Energy Conversion* in 2018 and a Prize Conference Paper Award at the Power and Energy Society General Meeting in 2022. She also co-authored the 2021 IEEE Power and Energy Society Prize Paper. Christine serves on the editorial boards of the *IEEE Transactions on Power Systems*, *IEEE Transactions on Energy Conversion*, and *IEEE PES Letters*.